

1  
2 **MAGMA STORAGE, ERUPTIVE ACTIVITY AND FLANK INSTABILITY: INFERENCES**  
3 **FROM GROUND DEFORMATION AND GRAVITY CHANGES DURING THE 1993-2000**  
4 **RECHARGING OF MT. ETNA VOLCANO**

5  
6  
7 Bonaccorso A., Bonforte A., Correnti G. , Del Negro C., Di Stefano A., Greco F.

8  
9 |  
10 Istituto Nazionale di Geofisica e Vulcanologia, Italy

11  
12  
13  
14 Submitted to  
15 Journal of Volcanology and Geothermal Research  
16 April 2010  
17

18  
19 Corresponding author

20  
21 Alessandro Bonaccorso

22  
23 Istituto Nazionale Geofisica e Vulcanologia

24 Sezione di Catania

25 Piazza Roma, 2

26 95123 Catania – Italy

27  
28 Ph. +39.095.7165800

29 Fax : +39.095.7165826

30 Email : [bonaccorso@ct.ingv.it](mailto:bonaccorso@ct.ingv.it)  
31  
32

33

34 **Abstract**

35

36 A long recharging period characterized Mount Etna volcano during 1993-2000 before the main  
37 explosive-effusive 2001 and 2002-03 flank eruptions. The joint analysis of ground deformation  
38 and gravity data over this entire period revealed that different phenomena occurred within Etna's  
39 plumbing system and clearly inferred two phases spanning 1993-97 and 1994-2000, respectively.  
40 The first phase was characterized by magma storage and accumulation at an intermediate depth  
41 (2-6 km below sea level), which provoked an overall inflation and positive gravity changes. During  
42 the second phase, the magma started to rise and intrude at shallower levels favouring the  
43 movement of the unstable eastern flank, which accelerated its sliding toward the East. The  
44 shallower magma accumulation also caused the gas exolution, associated with increasing  
45 explosive activity at the summit craters, detected by a gravity negative variation. The gravity  
46 measurements, independently of the same result obtained by geochemical studies, confirm that  
47 only 20-30% of the magma volumes supplied in the plumbing system were then erupted. The  
48 complex dynamic of rising magma beneath Mount Etna makes ground deformation and gravity  
49 measurements complementary, being able to detect different effects of magma emplacements  
50 beneath the surface. Our results also highlight how the joint use of ground deformation and  
51 gravity observations may be crucial in identifying the nature and rate of an impending season of  
52 volcanic eruptions.

53

54 **Keywords** : Etna, volcano, monitoring, deformation, gravity

55

56

57

## 58 1. Introduction

59

60 During recent decades, marked charging/discharging phases have been observed at Mount (Mt)  
61 Etna. The December 1991 – March 1993 lateral eruption, which represented the most important  
62 lateral eruption in the last three centuries both in terms of duration (472 days) and volume of  
63 erupted lava (about  $235 \times 10^6 \text{ m}^3$ ), was preceded by a dilatation trend measured by geodetic  
64 measurements since 1982 (Bonaccorso and Davis (2004), and was accompanied by an evident  
65 deflation (Bonaccorso, 1996; Puglisi et al., 2001) that indicated a depressurizing intermediate  
66 storage zone ca. 3 km below sea level (bsl) (Bonaccorso, 1996).

67 After the 1991-93 effusive eruption of Mt Etna, there began a new long recharging phase. The  
68 recharging phase was initially characterized by explosive manifestations from the end of 1995,  
69 when several strong lava fountain episodes occurred at summit craters. The volcanic activity took  
70 place principally at the North-East (NE) crater and preceded the resumption of activity at the  
71 South-East (SE) crater by about one year, which lasted almost continuously for the next four  
72 years. The second part of the recharging period was characterized by important events, such as  
73 the strong seismic swarms in January 1998 (Bonaccorso and Patanè, 2001) and April 2001 on the  
74 western flank, the subplinian explosion on 22 July 1998, the two sub-terminal eruptions (February-  
75 November 1999 and January 2001 eruptions) fed by the SE summit crater, and more than one  
76 hundred spectacularly explosive events of lava fountains and tephra emission from the SE summit  
77 crater during 2000-2001 (La Delfa et al., 2001; Alparone et al., 2003; Behncke and Neri, 2003;  
78 Bonaccorso, 2006), which characterized an unusual and very highly explosive period. The overall  
79 continuous recharging phase culminated with the two violent and dramatic explosive-effusive  
80 eccentric flank eruptions of July-August 2001 and October 2002 – January 2003 (e.g. Allard et al.,  
81 2006, Aloisi et al., 2006 and references hereinafter). The 2002-03 eruption was also characterized  
82 by a lateral effusive fissure propagating in the NE sector, which also promoted a marked  
83 acceleration of the eastward sliding of the volcano's south-eastern flank (e.g. Bonaccorso et al.,  
84 2006; Bonforte et al., 2007a; 2007b; 2008; Puglisi et al., 2008). These two flank eruptions marked  
85 a significant change in the volcano dynamic regime, and the study of the 1993-2000 preparatory  
86 recharging phase has a fundamental role for a deeper comprehension of the volcano's behaviour.  
87 During 1993-2000, the monitoring geophysical networks provided a multi-faceted reference data  
88 set that documented the recharging phase with considerable success. The seismicity pattern  
89 indicated a radial compression around an axial intrusion consistent with a pressurization at a  
90 depth of 6 to 15 kilometers, which triggered most of the seismicity (Patanè et al., 2003; Allard et  
91 al., 2006). Concurring with a pressurization phase, all geodetic measurements (EDM, GPS and  
92 InSar data) highlighted an overall continuous horizontal expansion of the volcano edifice from  
93 1993 to 2001. In spite of this nearly continuous expansion, the vertical pattern showed an overall  
94 uplift during 1993-1997 followed by lowering that affected mainly the south-eastern flank during  
95 1997-2000. The 1993-1997 period represented a net inflation of the volcano edifice and the  
96 deformation pattern pointed to a pressure source located at about 4 km bsl interpreted as an  
97 intermediate recharging magma storage (Bonaccorso et al., 2005).

98 Unlike the near-constant increasing horizontal expansion but similarly to the vertical up/down  
99 trend, the gravity data showed a reversal trend characterized by increase (1994-1997) decrease  
100 (1997-1999) cycle affecting mainly the central and eastern parts of the volcano and reaching a  
101 maximum amplitude of about 100  $\mu\text{Gal}$  peak-to-peak (Budetta et al., 1999; Carbone et al., 2003).  
102 The marked gravity changes cannot be justified by elevation changes, but could rather be due to  
103 the direct gravitational effect of magma accumulation and drainage below the volcanic pile.  
104 Significant gravity variations without ground height deformation have been reported at other  
105 volcanoes (Tiampo et al., 2004; Gottsmann et al., 2006; Hautmann et al., 2010), and thus different  
106 possible mechanisms to explain the increase/decrease gravity changes were explored.  
107 The uniqueness of the present work is twofold: (i) for the first time on Etna, the combined  
108 deformation and gravity datasets along a middle-term period (1993-2000) are investigated, and (ii)  
109 ground deformation and gravity data are systematically compared and the cross-related  
110 information obtained from the modeled sources is discussed.  
111 We highlighted that the entire 1993-2000 recharging period can be split in two main phases (1993-  
112 1997 and 1997-2000) due to different main sources. We show that the first one is due to a deeper  
113 magma storage and accumulation between 2-6 km below sea level, and the second is connected  
114 to the magma migration at shallower levels. We discuss how these sources are related to Etna's  
115 intermediate-shallow plumbing system, the explosive and eruptive activity, and the flank instability  
116 that characterized the eastern flank.

117

## 118 **2. Ground deformation during the 1993-2001 recharging phase**

119

120 Spanning/throughout the 1991-1993 eruption, Bonaccorso (1996) modeled a depressurizing  
121 ellipsoidal source located at about 3 km bsl depth. Just after the end of the 1991-1993 eruption,  
122 *Puglisi et al.*, (2001) modeled a pressurizing point source located again at about 3 km depth, by  
123 comparing the 1993 and 1994 GPS surveys, while no deep or significant shallow magmatic source  
124 apparently acted the following year (1994-1995) by analyzing GPS data (*Bonforte and Puglisi,*  
125 *2003*). InSAR data covering the same two-year period (1993-1995) led (*Lundgren, et al., 2003*) to  
126 model a pressurizing spheroidal cavity at a position very similar to the 1993-1994 GPS one. From  
127 1996 to 1997, the inflation phase underwent an acceleration as measured by GPS surveys (*Puglisi*  
128 *and Bonforte, 2004*).

129 During the entire 1993-2000 period, Mt Etna was affected by a continuous areal dilatation. EDM  
130 and GPS surveys, carried out at least yearly on the volcano, showed a marked areal dilatation of  
131 the measured networks, due to the radial spreading of the edifice (*Bonaccorso, et al., 2005;*  
132 *Bonforte and Puglisi, 2003; Puglisi and Bonforte, 2004, Puglisi et al., 2004; Houlié, et al., 2006b*).  
133 The GPS network is shown in Figure 1. From 1993, the GPS network on Mt Etna has been  
134 continuously improved, in order to cover a wider area and increase the spatial detail in ground  
135 deformation sampling. New benchmarks are constantly added above the volcano to improve the  
136 areal coverage and the spatial density of the network; furthermore, all new benchmarks are self-  
137 centering and some of them have been installed to replace older ones (nails), measured by tripods.

138 The new GPS network currently consists in several sub-networks: the main inner network, covering  
139 the volcano; the external reference frame, circling it on the stable sedimentary basement; the N-S  
140 profile, above 1800 m altitude and crossing the summit area; the E-W profile, at about 1800-2000  
141 m altitude across the southern flank; the “Ionica” network, lying over the entire eastern flank of Mt  
142 Etna below 1500 m altitude; two small networks, installed across the Pernicana fault (*Bonforte, et*  
143 *al., 2007a; Bonforte, et al., 2007b; Bonforte, et al., 2004; Puglisi and Bonforte, 2004; Puglisi, et al.,*  
144 *2008; Puglisi, et al., 2001*). In this paper, we consider data coming from the main inner network,  
145 from those stations having a significant historical record during the investigated period (1993-  
146 2000).

147 From 1993 to 2000, the areal dilatation showed a near-constant increasing trend which indicated a  
148 roughly continuous horizontal expansion of the volcano edifice (Fig. 2). The satellite interferometry  
149 InSar data also provided a coherent picture of the overall inflation, which characterized the volcano  
150 during 1993-2001 (Lanari et al., 1998; Lundgren et al., 2003; Neri et al., 2009).

151 However, a more detailed analysis of the displacement components shows that the vertical  
152 changes were characterized by an increasing/decreasing trend. During the entire 1993-2000  
153 expansion period, we can detect a first phase (1993-97) with vertical uplift (Fig. 3a) and a next  
154 phase (1997-2000) with a vertical lowering affecting mainly the south-eastern flank (Fig. 3b).

155 The geodetic measurements were focused on finding the ground deformation source acting  
156 beneath the volcano. Pressurizing sources were modeled during different periods.

157 The recharging phase spanning 1993-1997 represented a net inflation, not affected by significant  
158 volcanic activity as instead occurred from 1998. The deformation data recorded during the 1993-  
159 1997 inflation were inverted to model the pressuring intermediate storage by using analytical and  
160 numerical models with ellipsoidal pressuring source in elastic rheology that inferred a vertically  
161 elongated source with centre below the summit crater area at 4 km bsl (Bonaccorso et al., 2005).

162 After 1997, several eruptive phenomena occurred in the summit crater area. On 22 July 1998,  
163 powerful activity took place at central crater, with a sub-plinian paroxystic explosion; this activity  
164 produced a quick deflation of the edifice, detected by the tilt network. Modeling of tilt data  
165 indicated the fast depressurization of a source located at about 2-3 km bsl beneath the summit  
166 craters, i.e. shallower than the inferred pressurizing source (Bonaccorso, 2006).

167 In February 1999, a sub-terminal eruption started at the base of the SE summit crater and this  
168 magma output caused a slowing of the inflation rate during 1999, as revealed by the areal  
169 dilatation plot in Figure 2. After the end of this sub-terminal eruption, the volcano again began to  
170 dilate at a rate similar to that measured before 1999, and during 2000-2001 it was characterized  
171 by an extraordinary sequence of more than a hundred lava fountains from SE crater. A  
172 pressurizing source was modeled by *Puglisi et al., (2008)* using GPS and DInSAR data from 2000  
173 to 2001, located at 4 to 6 km bsl beneath the upper western flank of the volcano. Instead, *Houlié*  
174 *et al., (2006a; b)* inverted GPS data spanning the entire inflating phase of the volcano, from 1994  
175 to 2001, modeling a unique pressure source located at a depth of about 6 km bsl and  
176 representing an average of the different sources modeled by considering different shorter periods.

177

### 178 3. Gravity during the 1993-2001 recharging phase

179

180 The Etna gravity network for discrete measurements consists of 71 benchmarks distributed  
181 around the volcano and covers an area of about 400 km<sup>2</sup> (Fig. 1). Measurements over the entire  
182 Etna gravity network are usually repeated at six month to one-yearly intervals, although some  
183 parts of the array are reoccupied more frequently.

184 We analyze the microgravity data set spanning a 6-year period (1994-2000). The data were  
185 reduced for tidal effect and for instrumental drift, and were referred to Adrano (ADR) station, since  
186 it is the least likely station to be affected by volcanically-induced gravity changes (Budetta et al.,  
187 1999).

188

#### 189 3.1 Data

190

191 The elevation of each gravity station is not systematically monitored during the gravity surveys.  
192 Nevertheless, independent ground-deformation surveys provide enough data to evaluate Etna's  
193 vertical deformation with high detail. Using GPS data collected at stations very close to the gravity  
194 ones in the same period, gravity data were corrected for the free-air effect. We use the  
195 experimental free-air gravity gradient values observed at different gravity stations of the network  
196 to correct gravity data for height variations. Figure 4 shows several selected gravity sequences  
197 collected in different zones of the volcano compared with height variations at the closest GPS  
198 station, before and after the correction. The gravity and height variations are directly space-time-  
199 correlated (gravity increases with height), showing a similar up-down pattern for all the considered  
200 period (Fig. 4). However, height variations are too small to significantly affect surface gravity  
201 measurements and due to the directly correlation, after the free air correction, gravity sequences  
202 exhibit an even larger amplitude.

203 Despite the different sampling rate with which data are normally acquired on Etna, the height  
204 corrected gravity signals show two main long-term variations involving the different sectors of the  
205 volcano. A gravity increase starting during the last months of 1995 and culminating at the end of  
206 1996, when it reached a maximum amplitude of about 100  $\mu$ Gal in the stations located on the  
207 southeastern flank and on the summit of the volcano. The apparent shift in time of the positive  
208 cycle (Fig. 4), which seems to exist between data sequences from different zones, could be, at  
209 least in part, the effect of the different sampling rate. At the end of 1997, the gravity field inverted  
210 its trend and in late-1998 reached a minimum level (about -110  $\mu$ Gal) lower than it was in 1993,  
211 before the increase took place. The gravity changes at stations very far from the summit craters (>  
212 15 km) remain within 20  $\mu$ Gal peak-to-peak during the entire period especially in the West and  
213 North flanks (Fig. 4). The seasonal effects can be considered negligible, since the selected gravity  
214 variations have been extracted from the entire data set at approximately the same time every year.  
215 To show how the 1994-1997 (positive trend) and 1997-1999 (negative trend) gravity changes are  
216 distributed over space, the height corrected gravity data acquired in 34 gravity benchmarks from  
217 the entire Etna network were contoured over two time intervals (Fig. 5a, b). Both gravity contour

218 maps clearly show how the positive (Fig. 5a) and negative (Fig. 5b) gravity variations, identified by  
219 the different sectors of the volcano, are distributed around the volcano with a wavelength of about  
220 10÷12 km, affecting mainly the central and eastern zones, indicating also an absence of significant  
221 gravity variations elsewhere within the gravity network.

222

### 223 *3.2 Gravity Modeling*

224

225 The data sets from the entire Etna network were separately modeled for the 1993-1997 increase  
226 and 1997-1999 decrease to infer the gravity source. In order to model the observed gravity  
227 changes, we firstly investigate if the deformation source detected by geodetic data inversion  
228 (Bonaccorso et al., 2005) could justify the increase (1993-1997) and decrease (1997-1999) in the  
229 observed gravity field. The wavelength of the microgravity observations did not support the  
230 presence of mass redistribution at the depth of the proposed ellipsoidal source (Budetta et al.,  
231 1999; Currenti et al., 2007). Both the amplitude and the extent of the observed gravity changes  
232 point to a shallower gravity source with respect to the ground deformation one. Thus we analyzed  
233 the possible source that could produce the observed gravity changes.

234 The observed gravity changes and ground uplift are unusually positively correlated. Although  
235 positive gravity changes are usually thought to indicate ground subsidence, the GPS  
236 measurements revealed an overall uplift. The large gravity increase during 1993-1997  
237 accompanied by slight height changes, could be attributed to a storage of new mass beneath the  
238 volcano. In order to evaluate the characteristics of the source that caused the observed gravity  
239 changes, we investigated four models with different source geometries: sphere, prism, cylinder,  
240 and ellipsoid. We inverted the recorded gravity changes applying a Genetic Algorithm optimization  
241 procedure, searching for the source parameters that minimize the misfit between the observed and  
242 computed gravity changes (Carbone et al., 2008). As forward model, we used the analytical  
243 solutions for all the source geometries (Singh, 1977; Clark et al., 1986; Blakely 1996) and included  
244 the topography, taking into account the altitude difference between the gravity station and the  
245 source. The results show that, despite the different geometries, all the sources can reproduce the  
246 observed anomaly with a misfit lower than 20  $\mu\text{Gal}$  (Table 1). As an example, we report the case of  
247 a simple spherical source located at 1820 m bsl that is able to reproduce the observed gravity  
248 anomaly (Fig. 6). The estimated mass change is linearly related to the density contrast and the  
249 volume, with a smaller density contrast yielding a larger source radius and vice versa. Thus we  
250 avoided the ambiguity inverting only the value of the mass change obtaining a value of about  
251  $320 \times 10^9$  kg. Employing a model based on a prismatic source, we found that the observed gravity  
252 change is best explained with a source located at a depth of 2160 m bsl, with a length of 2880 m,  
253 width of 1770 m and orientation NW-SE. The calculated anomaly depends on both the density  
254 contrast between the source and the surrounding rocks and the thickness of the source, thus we  
255 invert the product  $U \cdot \Delta\rho$  as source parameter. The estimated mass change,  $340 \times 10^9$  kg, is  
256 comparable to the previous case. Considering an elongated conduit of radius 310 m, height 3320  
257 m and depth of the centre 2480 m bsl, we model the observed anomaly with a similar misfit and

258 estimated mass change. Finally, we applied an ellipsoidal source and the best fit to the recorded  
259 data is given for a source located at a depth of 2300 m bsl, with the major semi-axis of 1360 m and  
260 the other two semi-axis of 300 m. In this case, a density contrast of  $390 \text{ kg/m}^3$  is necessary to  
261 justify the measured gravity change. All the geometries represent plausible sources of the  
262 observed anomaly, since potential field measurements cannot unambiguously identify the shape of  
263 the source at depth. The inferred horizontal location for all the geometries is similar to the  
264 deformation source for the same period, whereas the depth of the mass centre ranges between  
265 1800 m and 2500 m bsl. The calculations show a mass increase of about  $300 \times 10^9 \text{ kg}$ , which yields  
266 at least a source volume of about  $800 \times 10^6 \text{ m}^3$  considering a density contrast of  $400 \text{ kg/m}^3$ .  
267 During 1997-1999, the similarity in wavelength and position of the negative gravity anomaly with  
268 respect to the previous gravity increase reflects a mass decrease likely to take place within the  
269 same source. The gravity decrease can be modeled with the same source used to justify the  
270 gravity increase (Table 1), assuming the value of mass change to be opposite in sign with respect  
271 to the first period.

272

## 273 **4. Discussion**

274

### 275 *4.1 The Etna plumbing system and the two main phases of the 1993-2000 recharging period*

276

277 After the 1991-93 eruption, the ground deformation and gravity data univocally indicated that the  
278 following 1993-2000 recharging process at Mt Etna occurred in two main phases.

279 The first phase, from 1993 (just after the end of the eruption) to 1997, was characterized by the  
280 continuous pressurization of the feeding system of the volcano. In this interval, the ground  
281 deformation modeling infers a vertically elongated pressurizing source centered about 4 km bsl  
282 (Bonaccorso et al., 2005). Moreover, we showed that the positive gravity anomaly can be modeled  
283 with a mass accumulation centered at about 1.5 – 2 km bsl. Both gravity data and ground  
284 deformation presented in this paper and reported by literature contribute in identifying the shallow-  
285 intermediate magma plumbing system. At intermediate depth (2-6 km bsl), it is composed of a  
286 vertically elongated storage volume that bounds the western side of the high-velocity body (HVB)  
287 detected by seismic tomography (Patanè et al., 2003). This intermediate elongated pressurizing  
288 storage provokes a wide ground deformation pattern as revealed by the terrestrial and satellite  
289 geodetic measurements (Fig. 3a). Then most of the magma mass is cumulated at the shallower  
290 interface of the upper limit of the HVB and is detected by the gravity changes, which consequently  
291 affected a smaller/narrower area (Fig. 5a). The HVB is a large plutonic body, probably composed  
292 of frozen dykes, with bottom at a depth of about 18 km as clearly revealed by seismic tomography  
293 (e.g. Hirn et al., 1991; Chiarabba et al., 2000). Its estimated volume is about 3-4 times larger than  
294 the volcano pile, and its accretion has recently been considered as a possible cause that  
295 destabilizes the eastern flank (Allard et al., 2006). The sliding of the eastern flank has been  
296 investigated by different geological and structural studies since the 90s (e.g. Lo Giudice and Rasà  
297 Rust, 1986; Borgia et al., 1992; Rust and Neri, 1996), and more recently measured in detail by



298 several deformation studies (see Bonaccorso et al., 2006 and references hereinafter). The 1993-97  
299 pressurization phase was characterized by a fairly continuous increase in the gravity field and an  
300 overall inflation of the volcano, with horizontal expansion and diffuse uplift. Only two GPS stations,  
301 on the middle and lower eastern flank of the volcano showed subsidence, revealing a first  
302 expression of an incipient seawards motion of this side of Mt Etna (Fig. 3a).

303 During the second phase, after 1997 until 2000, the volcano showed a more complex behavior.  
304 Indeed, gravity data showed a progressive decrease while geodetic data continued to measure a  
305 horizontal expansion as shown by the areal dilatation (Fig. 2) and GPS horizontal radial  
306 displacements (Fig. 3). However, the ground deformation pattern is complicated by a general  
307 subsidence of GPS stations (Fig. 3b), the reverse to the uplift previously measured, but well  
308 correlated to the gravity trend (Fig. 4). This subsidence mainly affected all the stations lying on the  
309 eastern side of the volcano, while stations on the western and northern stable sides showed largely  
310 horizontal radial motions with less significant vertical displacements.

311

#### 312 *4.2 Magma movement: stored and erupted volumes*

313

314 During 1994-1997, the positive gravity changes indicate a cumulated mass of about  $800 \times 10^6 \text{ m}^3$ ,  
315 while the extruded magma during the recharging phase and the following 2001 and 2002-2003 is  
316 about  $200 \times 10^6 \text{ m}^3$  (Table 2). Therefore during the period 1993-2003, which comprises the  
317 recharging plus discharging phases, there are 4 times more accumulating than erupted magma.  
318 This geophysical result agrees fairly well with the geochemistry constraints on mass accumulation  
319 and discharging. In fact, based on measured volcanic  $\text{SO}_2$  flux, at Etna the ratio between  
320 degassed magma and extruded magma was calculated at about 4 in the period 1975-1995 (Allard,  
321 1997) and about 3.3 in the period 1993–2004 (Allard et al., 2006). Therefore, gravity  
322 measurements independently confirm that only 20-30% of the magma volumes supplied and  
323 cumulated in the plumbing system were then erupted. The general mechanism to explain the  
324 higher quantity of degassing magma is convective ascent and recycling (e.g. Kazahaya et al.,  
325 1994; Stevenson and Blake, 1998). The non-degassed magma travels up the volcanic edifice; at  
326 shallower depth the gases are released through vesiculation process and then the denser  
327 degassed magma descends in the volcanic feeding system.

328 This mechanism has also been proposed at Etna to explain the predominant quantity of un-erupted  
329 degassed magma (Allard, 1997). Furthermore, Allard (1997) proposes the wide plutonic body to be  
330 the final destination for the un-erupted magma, which thus contributes to the accretion of wide  
331 plutonic roots in the basement of Etna. Following this view and in accordance with Carbone et al.  
332 (2003), since most of the estimated magma has not been erupted (70-80%), it could have been  
333 recycled by the Etna plumbing system, sinking down to a deeper level, increasing and pushing the  
334 plutonic body in the Etna's basement. However, the possible gravity effect due to this scenario  
335 would cover a greater distance than the total extent of our network and thus would be beyond the  
336 limits of detection by the gravity surveys.

337 The exolution of the principal gases present in Etnean magmas begins at pressures of about 100-  
338 140 MPa (~ 3 - 4 km lithostatic depth), up to 10 MPa (Spilliaert et al., 2006). During its ascending  
339 path along the feeding system of the volcano, magma passed beyond the gas exolution depth and  
340 began to further vesiculate following the above considerations. Progressive vesiculation and  
341 volatile exolution, owing to the reduction of lithostatic pressure, induces significant decreases in the  
342 bulk density of the mixture of bubbles and liquid magma (Sparks, 1978). As calculated by Corsaro  
343 and Pompilio (2003), vesiculation process of magma could reduce its density up to 25%; such a  
344 density reduction on the magma storage modeled beneath the volcano is able to produce a  
345 consistent part of the gravity decrease measured from 1997 to 1999, and promote the convective  
346 magma movements. In addition, the hypothesis proposed by Carbone et al. (2009) of the rock  
347 rarefaction due to the extension and micro-fracturing induced by flank movement has to be taken  
348 into account and could further contribute to the gravity decrease. This schematic evolution also  
349 concurs well with the volcanic activity observed at summit craters of the volcano; indeed, after  
350 1998, stronger explosive activity took place, starting from a sub-plinian eruption at the central  
351 crater in July 1998, whose source has been modeled by Bonaccorso (2006) at about 2.5 km bsl,  
352 which is shallower than the 1993-97 deformation source and at a similar depth to the modeled  
353 gravity source. In February 1999, a sub-terminal eruption started at the base of SE Crater at 2900  
354 m of altitude lasting ten months, and strong strombolian activity took place at Bocca Nuova crater  
355 lasting until 2000, when also a total of a hundred spectacular lava fountains took place at SE crater  
356 till June 2001. This kind of activity well testifies the strong and violent degassing of the magma  
357 stored, confirming the hypothesis of the strong vesiculation process occurring along the feeding  
358 system of the volcano.

359

#### 360 *4.3 Flank instability*

361

362 As already evidenced by several studies, we usually observe a dual dynamics on Etna: a deeper  
363 one related to magma movement in the crust; a shallower one related to flank sliding. In agreement  
364 with literature, we consider that magma rises from depth along the NW border of the HVB (Patanè  
365 et al., 2003), where all pressure sources are detected (see Bonforte et al., 2008 for a review). At  
366 those intermediate depths, magma storage produces detectable ground deformation. The vertical  
367 deformation pattern suggests that the flank instability, that was affecting only the lowermost part  
368 from 1993 to 1997, extended to involve the entire unstable eastern flank of the volcano after 1997.  
369 The dip angles of the displacement vectors reported in the E-W cross section (Fig. 3b), decreasing  
370 from the central part to the eastern periphery, makes the rotational slope failure kinematics of the  
371 entire eastern flank evident. The continuous and strong inflation from 1993 to 1997 induced a  
372 radial expansion of the volcano. This expansion promoted the instability of the eastern un-  
373 buttressed flank with a consequent first seawards motion (Fig. 3a, 7a).

374 The seawards motion triggered a feedback process between magma uprising and gravitational  
375 sliding (Walter et al., 2005). The sliding favoured an extension and depressurization on the central  
376 part of the volcano facilitating magma ascent at shallower levels filling the main conduit and

377 producing also the first attempts of lateral intrusions as detected in 1998 (Bonaccorso and Patanè,  
378 2001); these intrusions, in turn, produced additional stress at shallow depth favoring the instability  
379 of the un-buttressed side of the volcano (Fig. 3b, 7b).

380 The mass accumulation, detected by gravity data, is located at the top of the rigid HVB at the same  
381 depth of the sub-horizontal sliding surface modeled by *Bonforte and Puglisi* (2003; 2006) by  
382 ground deformation data. In these conditions, magma movements at those depths do not produce  
383 significant mass variations, due to the very small density contrast between magma and  
384 surrounding rocks. At the shallower levels, i.e. over the upper limit of the HVB, the cumulating  
385 magma can push the shallower and more unstable eastern flank (Fig. 3b, 7b), This dynamics does  
386 not allow strong pressurization, since most of the deformation produced by magma emplacement  
387 is accommodated by the displacement of the eastern side which moves downslope, provoking an  
388 extensional zone at the top of the HVB. Such non-elastic conditions produce a detectable mass  
389 accumulation with less significant ground deformation. The opposite dynamic conditions during  
390 magma upraise beneath Mt Etna makes ground deformation and gravity measurements highly  
391 complementary, being able to detect different effects of magma emplacements beneath the  
392 surface, as evidenced by (*Bonforte, et al.*, 2007b) in the case of the 2002-2003 dyke emplacement.

393

## 394 **5. Conclusion**

395

396 During 1993-2000, a marked recharging phase of Mt Etna preceded the main effusive-explosive  
397 lateral eruptions of 2001 and 2002-03. The deformation and gravity patterns provide powerful  
398 indications on the magma supply and accumulation mechanisms at Etna.

399 Both methodologies highlight that the entire 1993-2000 inflation can be divided into two main  
400 phases showing different deep and shallow dynamics of the volcano. The first one from 1993 to  
401 1997 was characterized by the pressurization of the deeper feeding system and magma  
402 accumulation at 2÷6 km depth. The magma storage occurred at the north-western side of the high  
403 velocity body (HVB) and also on its top, where also the decollement of the eastern flank occurs. In  
404 this period, only the lower part of the eastern flank showed a first sliding movement. The magma  
405 storage pressurization provoked both an inflation and a positive gravity change due to mass  
406 accumulation. The second period from 1997 to 2000 was characterized by the upraise of magma  
407 from the deeper source towards the surface. The magma upraise within the shallow plumbing  
408 system of the volcano was accompanied by the accelerated sliding dynamic of the eastern flank as  
409 observed by geodetic measurements. In the same period, the magma migration at shallower levels  
410 produced the gas exolution feeding the reinforced volcanic and explosive activity at summit craters.  
411 The observed decrease in gravity was consistent with this process. In agreement with previous  
412 geochemistry results, the magma volume estimated from the gravity changes during the 1993–  
413 1997 is about 3.3 - 4 times higher than the magma erupted during the 1997–2003 period. We  
414 deduce that the mass decrease measured during the second period may reasonably be imputed to  
415 vesiculation and magma recycling in the deep feeding system.

416 A novelty revealed by the combined analysis of ground deformation and gravity data over the long  
417 inflating period from 1993 to 2000 is the correlation among the change in the kinematics of the  
418 eastern flank of the volcano, the gravity variations, the vertical motions and the eruptive activity.  
419 In this paper, an effort was made in order to give an overall picture of the deep and shallow  
420 phenomena occurring beneath Mt Etna through ground and gravity observations. Despite the  
421 difficulties in interpreting these data jointly, the results are encouraging since the complementarity  
422 of these two approaches helps to better understand some mechanisms that precede and  
423 accompany volcanic eruptions, crucial to minimize their hazard.

424  
425

## 426 **References**

- 427 Allard, P., 1997. Endogenous magma degassing and storage at Mount Etna, *Geophys. Res. Lett.*, 24, 2219–  
428 2222.
- 429 Allard, P., Behncke, B., D'Amico, S., Neri, M., Gambino, S., 2006. Mount Etna 1993–2005: Anatomy of an  
430 evolving eruptive cycle, *Earth Sci. Rev.* 78, 85–114.
- 431 Aloisi, M., Bonaccorso, A., Gambino, S., 2006. Imaging composite dike propagation (Etna 2002, case), *J.*  
432 *Geophys. Res.*, 111, B06404, doi:10.1029/2005JB003908.
- 433 Alparone, S., Andronico, D., Lodato, L., Sgroi, T., 2003. Relationship between tremor and volcanic activity  
434 during the Southeast Crater eruption on Mount Etna in early 2000, *J. Geophys. Res.* 108, 2241.  
435 doi:10.1029/2002JB001866.
- 436 Blakely, R.J., 1995. *Potential Theory in Gravity and Magnetic Applications*, Cambridge University Press, New  
437 York, 1995.
- 438 Behncke, B., Neri, M., 2003. Cycles and trends in the recent eruptive behaviour of Mount Etna (Italy),  
439 *Canadian J. Earth Sci.* 40, 1405-1411, doi: 10.1139/E03-052.
- 440 Bonaccorso, A., 1996. Dynamic inversion of ground deformation data for modelling volcanic sources (Etna  
441 1991-93), *Geophysical Research Letters*, 23, 451-454.
- 442 Bonaccorso, A., 2006. Explosive activity at Mt. Etna summit craters and source modeling by using high  
443 precision continuous tilt. *Journal of Volcanology and Geothermal Research*, 221-234, 158,  
444 doi:10.1016/j.jvolgeores.2006.05.007
- 445 Bonaccorso, A., Patanè, D., 2001. Shear response to an intrusive episode at Mt Etna volcano (January  
446 1998) inferred through seismic and tilt data, *Tectonophysics*, 334, 61-75.
- 447 Bonaccorso, A., Davis, P.M., 2004. Modeling of ground deformation associated with recent lateral eruptions:  
448 Mechanics of magma ascent and intermediate storage at Mt.Etna, in *Etna Volcano Laboratory*,  
449 *Geophys. Monogr. Ser.*, vol. 143, Eds A. Bonaccorso, S. Calvari, M. Coltelli, C. Del Negro and S.  
450 Falsaperla, pp. 293-306, AGU, Washington, D. C.
- 451 Bonaccorso, A., Cianetti, S., Giunchi, C., Trasatti, E., Bonafede, M., Boschi, E., 2005. Analytical and 3-D  
452 numerical modelling of Mt. Etna (Italy) volcano inflation, *Geophys. J. Int.*, 163, 852–862, doi:  
453 10.1111/j.1365-246X.2005.02777.x
- 454 Bonaccorso, A., Bonforte, A., Guglielmino, F., Palano, M., Puglisi, G., 2006. Composite ground deformation  
455 pattern forerunning the 2004–2005 Mount Etna eruption, *J. Geophys. Res.*, 111, B12,  
456 doi:10.1029/2005JB004206.

457 Bonforte, A., Puglisi, G., 2003. Magma uprising and flank dynamics on Mount Etna volcano, studied using  
458 GPS data (1994-1995), *Journal of Geophysical Research-Solid Earth*, 108, B3,  
459 doi:10.1029/2002jb001845.

460 Bonforte, A., Puglisi G., 2006. Dynamics of the eastern flank of Mt Etna volcano (Italy) investigated by a  
461 dense GPS network, *Journal of Volcanology and Geothermal Research*, 153, 357-369, doi:  
462 10.1016/j.jvolgeores.2005.12.005.

463 Bonforte, A., Bonaccorso A., Guglielmino F., Palano M., Puglisi G., 2008. Feeding system and magma  
464 storage beneath Mt Etna as revealed by recent inflation/deflation cycles, *Journal of Geophysical*  
465 *Research-Solid Earth*, 113, B05456, doi:10.1029./2007JB005334

466 Bonforte, A., Branca, S., Palano, M., 2007a. Geometric and kinematic variations along the active Pernicana  
467 fault: Implication for the dynamics of Mount Etna NE flank (Italy), *Journal of Volcanology and Geothermal*  
468 *Research*, 160, 210-222, doi:10.1016/j.jvolgeores.2006.08.009.

469 Bonforte, A., Carbone, D., Greco, F., Palano, M., 2007b. Intrusive mechanism of the 2002 NE-rift eruption at  
470 Mt Etna (Italy) modelled using GPS and gravity data. *Geophys. J. Int.*, 169, 339–347, doi: 10.1111/j.1365-  
471 246X.2006.03249.x.

472 Bonforte, A., Guglielmino, F., Palano, M., Puglisi, G., 2004. A syn-eruptive ground deformation episode  
473 measured by GPS, during the 2001 eruption on the upper southern flank of Mt Etna, *Bulletin of*  
474 *Volcanology*, 66, 336-341, doi: 10.1007/s00445-003-0314-x

475 Borgia, A., Ferrari, L., Pasquarè, G., 1992. Importance of gravitational spreading in the tectonic and volcanic  
476 evolution of Mount Etna. *Nature* 357: 231-235.

477 Budetta G., Carbone, D., Greco, F., 1999. Subsurface mass redistributions at Mount Etna (Italy) during the  
478 1995-96 explosive activity detected by microgravity studies. *Geoph. J. Int.*, 138, 77-88.

479 Carbone, D., Budetta, G., Greco, F., 2003. Bulk processes prior to the 2001 Mount Etna eruption, highlighted  
480 through microgravity studies. *J. Geophys. Res.* 108. doi:10.1029/ 2003JB002542.

481 Carbone, D., Currenti, G., Del Negro, C., 2008. Multi-objective genetic algorithm inversion of ground  
482 deformation and gravity changes spanning the 1981 eruption of Etna volcano. *J. Geophys. Res.*, 113,  
483 B07406, doi:10.1029/2006JB004917.

484 Carbone, D., D'Amico, S., Musumeci, C., Greco, F., 2009. Comparison between the 1994 2006 seismic and  
485 gravity data from Mt Etna: new insight into the long-term behavior of a complex volcano. *Earth Planet.*  
486 *Sci. Lett.* 279, 282292.

487 Chiarabba, C., Amato, A., Boschi, E., Barberi, F., 2000. Recent seismicity and tomographic modeling of the  
488 Mount Etna plumbing system, *J. Geophys. Res.* 105, 10923-10938.

489 Clark, D.A., Saul, S.J., Emerson, D.W., 1986. Magnetic and gravity anomalies of a triaxial ellipsoid.  
490 *Exploration Geophysics* 17, 189-200.

491 Coltelli M., Proietti, C., Branca, S., Marsella, M., Andronico, D., Lodato, L., 2007. Analysis of the 2001 lava  
492 flow eruption of Mt. Etna from three-dimensional mapping, *J. Geophys. Res.*, 112, F02029,  
493 doi:10.1029/2006JF000598.

494 Corsaro, R.A., Pompilio, M., 2004. Buoyancy-controlled eruption of magmas at Mt Etna, *Terra Nova* 16, 16-  
495 22.

496 Currenti, G., Del Negro, C., Ganci, G., 2007. Modelling of ground deformation and gravity fields using finite  
497 element method: an application to Etna volcano, *Geophysical Journal International*, 169, 775-786.

498 Gottsmann, J., Wooller, L.K., Marti, J., Fernandez, J., Camacho, A.G., Gonzalez, P., Garcia, A., Rymer, H.,  
499 2006. New evidence for the reactivation of Teide Volcano. *Geophys. Res. Lett.* 33.  
500 doi:10.1029/2006GL027523.

501 Hautmann, S., Gottsmann J., Camacho A.G., Fournier N., Sacks I.S., Stephen R. , Sparks, J., 2010. Mass  
502 variations in response to magmatic stress changes at Soufriere Hills Volcano, Montserrat (W.I.): Insights  
503 from 4-D gravity data. *Earth and Planetary Science Letters*, 290 (2010) 8389.

504 Hirn, A., Nercessian, A., Sapin, M., Ferrucci, F., Wittlinger, G., 1991. Seismic heterogeneity of Mt Etna:  
505 structure and activity, *Geophys. J. Int.*, 105, 139–153.

506 Houlie, N., Briole, P., Bonforte, A., Puglisi, G., 2006a. Large scale ground deformation of Etna observed by  
507 GPS between 1994 and 2001, *Geophysical Research Letters*, 33, 2, L02309, doi: 10.1029/2005gl024414.

508 Houlie, N., Briole, P., Bonforte, A., Puglisi, G., 2006b. Large scale ground deformation of Etna observed by  
509 GPS between 1994 and 2001 (vol 33, art no L02309, 2006), *Geophysical Research Letters*, 33, 20,  
510 L20309, doi: 10.1029/2006gl026892.

511 Kazahaya, K., Shinohara, H., Uto, K., Odai, M., Nakahori, Y., Mori, H., Iino, H., Miyashita, M., Hirabayashi, J.  
512 2004. Gigantic SO<sub>2</sub> emission from Miyakejima volcano, Japan, caused by caldera collapse, *Geology*, 32,  
513 425-428, doi: 10.1130/G20399.1.

514 La Delfa, S., Patane', G., Clocchiatti, R. Joron, J.L., Tanguy J.C., 2001. Activity of Mount Etna preceding the  
515 February 1999 fissure eruption: inferred mechanism from seismological and geochemical data, *J. Volc.  
516 Geotherm. Res.*, 105, 121–139.

517 Lanari, R., Lundgren, P., Sansosti, E., 1998. Dynamic deformation of Etna volcano observed by satellite  
518 radar interferometry, *Geophys. Res. Lett.*, 25, 1541–1544.

519 Lo Giudice, E., Rasa', R., 1986. The role of the NNW structural trend in the recent geodynamic evolution of  
520 North-Eastern Sicily and its volcanic implications in the Etnean area, *J. Geodyn.*, 5, 309–330.

521 Lundgren, P., Berardino, P., Coltelli, M., Fornaro, G., Lanari, R., Puglisi, G., Sansosti, E., Tesauro, M., 2003.  
522 Coupled magma chamber inflation and sector collapse slip observed with synthetic aperture radar  
523 interferometry on Mt Etna volcano, *Journal of Geophysical Research-Solid Earth*, 108, B5, doi:  
524 10.1029/2001jb000657.

525 Neri, M., Casu, F., Acocella, V., Solaro, G., Pepe, S., Berardino, P., Sansosti, E., Caltabiano, T., Lundgren,  
526 P., Lanari, R., 2009. Deformation and eruptions at Mt. Etna (Italy): A lesson from 15 years of  
527 observations, *Geophys. Res. Lett.*, 36, L02309, doi:10.1029/2008GL036151

528 Palano, M., Gresta, S., Puglisi, G., 2008. Ground deformation patterns at Mt. Etna from 1993 to 2000 from  
529 joint use of InSAR and GPS techniques, *J. Volcanol. Geotherm. Res.* 169, 99–120.

530 Patanè, D., De Gori, P., Chiarabba, C., Bonaccorso, A., 2003. Magma ascent and the pressurization of  
531 Mount Etna's volcanic system, *Science*, 299, 2061-2063.

532 Puglisi, G., Bonforte, A., 2004. Dynamics of Mount Etna Volcano inferred from static and kinematic GPS  
533 measurements, *Journal of Geophysical Research-Solid Earth*, 109, B11, doi:10.1029/2003jb002878.

534 Puglisi, G., Bonforte, A., Maugeri, S.R., 2001. Ground deformation patterns on Mount Etna, 1992 to 1994,  
535 inferred from GPS data, *Bulletin of Volcanology*, 62, 371-384.

536 Puglisi, G., Briole, P., Bonforte, A., 2004. Twelve years of ground deformation studies on Mt. Etna volcano  
537 based on GPS surveys, in *Etna Volcano Laboratory, Geophys. Monogr. Ser., vol. 143*, Eds A.  
538 Bonaccorso, S. Calvari, M. Coltelli, C. Del Negro and S. Falsaperla, pp. 321-341, AGU, Washington,  
539 D. C.

540 Puglisi, G., Bonforte, A., Ferretti, A., Guglielmino, F., Palano, M., Prati, C., 2008. Dynamics of Mount Etna  
541 before, during, and after the July-August 2001 eruption inferred from GPS and differential synthetic  
542 aperture radar interferometry data, *Journal of Geophysical Research-Solid Earth*, 113, B06405,  
543 doi:10.1029/2006jb004811

- 544 Rust, D., Neri, M., 1996. The boundaries of large-scale collapse on the flanks of Mount Etna, Sicily, in  
545 *Volcano instability on the Earth and other planets*, *Geol. Soc. Spec. Publ. 110*, edited by W. J.  
546 McGuire, A. P. Jones, and J. Neuberg, pp. 193-208.
- 547 Singh, S. K., Gravitational attraction of a vertical right circular cylinder, *Geophys. J. R. Astron. Soc.*, 50, 243-  
548 246, 1977.
- 549 Sparks, R.S.J., 1978. The dynamics of bubble formation and growth in magmas: a review and analysis, *J.*  
550 *Volcanol. Geotherm. Res.* 3, 1–37.
- 551 Spilliaert, S., Metrich, N., Allard, P., 2006. S-Cl-F degassing pattern of water-rich alkali basalt: Modelling and  
552 relationship with eruption styles on Mount Etna volcano. *Earth Planetary Science Letters*, 248, 772-786.
- 553 Stevenson, D., Blake, S., 1998. Modelling the dynamics and thermodynamics of volcanic degassing, *Bulletin*  
554 *of Volcanology* **60**, pp. 307–317
- 555 Tiampo, K.F., Fernandez, J., Jentsch, G., Charco, M., Rundle, J.B., 2004. New results at Mayon, Philippines,  
556 from a joint inversion of gravity and deformation measurements. *Pure Appl. Geophys.* 161, 14331452.
- 557 Walter, T.R., Acocella, V., Neri, M., Amelung, F., 2005. Feedback processes between magmatic events and  
558 flank movement at Mount Etna (Italy) during the 2002–2003 eruption, *J. Geophys. Res.*, 110, B10205,  
559 doi:10.1029/2005JB003688

560

561

## 562 **Acknowledgements**

563 This study was undertaken with financial support from the V3-LAVA and V4-FLANK projects (DPC-INGV  
564 2007-2009 contract).

565

566 **Captions**

567

568

569

570

571

572

573

574

575

576

577

578

579

**Figure 1.** Map showing the position of the height corrected gravity benchmarks of Etna's microgravity network (red triangles) and the GPS benchmarks (black circles). Dashed line contours the seawards moving flank of the volcano. The inset at the top left shows the location of Etna volcano with respect to Sicily, the one at the bottom left shows the position of the four Summit Craters (NEC = Northeast Crater, VOR = Voragine, BNC = Bocca Nuova, SEC = Southeast Crater). The benchmarks are grouped in different areas (shaded green squares numbered from 1 to 6; 1 North Zone, 2 North East Zone, 3 South East Zone, 4 South West Zone, 5 West Zone and 6 Summit Zone). The signals of the labeled gravity and GPS benchmarks within each zone are presented in Figure 4. Geographical coordinates are expressed in UTM projection, zone 33N.

580

581

582

**Figure 2.** Cumulative areal dilatation calculated since 1990 for the area covered by the GPS network.

583

584

585

586

**Figure 3.** Map and section of the displacements measured in the intervals 1993-1997 (a) and 1997-2000 (b), respectively. The area within the dashed white square is covered by the gravity contour maps shown in Figure 5a, b.

587

588

589

590

**Figure 4.** Selected gravity signals collected in different areas (labeled in Figure 1) of the volcano from 1993 to 2000 compared with height variations at the closest GPS station, before and after the free air correction.

591

592

593

**Figure 5.** Sketch maps showing gravity changes for the (a) July 1994 – June 1997 (gravity increase) and (b) June 1997 – June 1999 (gravity decrease) periods.

594

595

596

597

**Figure 6.** Gravity changes expected from a spherical source located under crater area at 1820 bsl. Different geometries can reproduce a similar pattern (see Table 1 for the complete parameters of the sources).

598

599

600

601

602

603

604

605

606

607

608

609

**Figure 7.** Sketch map of the main phases during the 1993-2000 recharging. Magma rises from the deeper levels (1) along the western border of the high velocity body (HVB). At intermediate depth of about 4 km bsl, the magma is stored in a vertically elongated source (2) located in the upper western border of the HVB as inferred by ground deformation modeling. The pressurization of this source provokes a near-continuous expansion of the volcano edifice. (A) During 1993-1997, magma is also accumulated along the upper limit of the VHD (3) as inferred by the gravity changes pattern. In this period, a first sliding toward the East was recorded in the lowermost part of eastern flank through sliding planes modeled in previous studies (see references in the text). (B) During 1997-2000 the gases are released, a high explosivity characterized this period; then the denser degassed magma descended in the volcanic feeding system provoking a gravity decrease.

610

611

**Table 1 -** Source parameters inferred from inversion of gravity data.

612

613

614

615

**Table 2 -** Magma erupted volumes during the period 1993-2004 after Benchke and Neri (2003), Allard et al. (2006) and Coltelli et al. (2007). The estimated volumes take into account both lava (emitted from effusive eruptions, lava flows from eruptive episodes and overflows from central craters) and tephra (emitted from explosive activity).



Figure 1  
[Click here to download high resolution image](#)

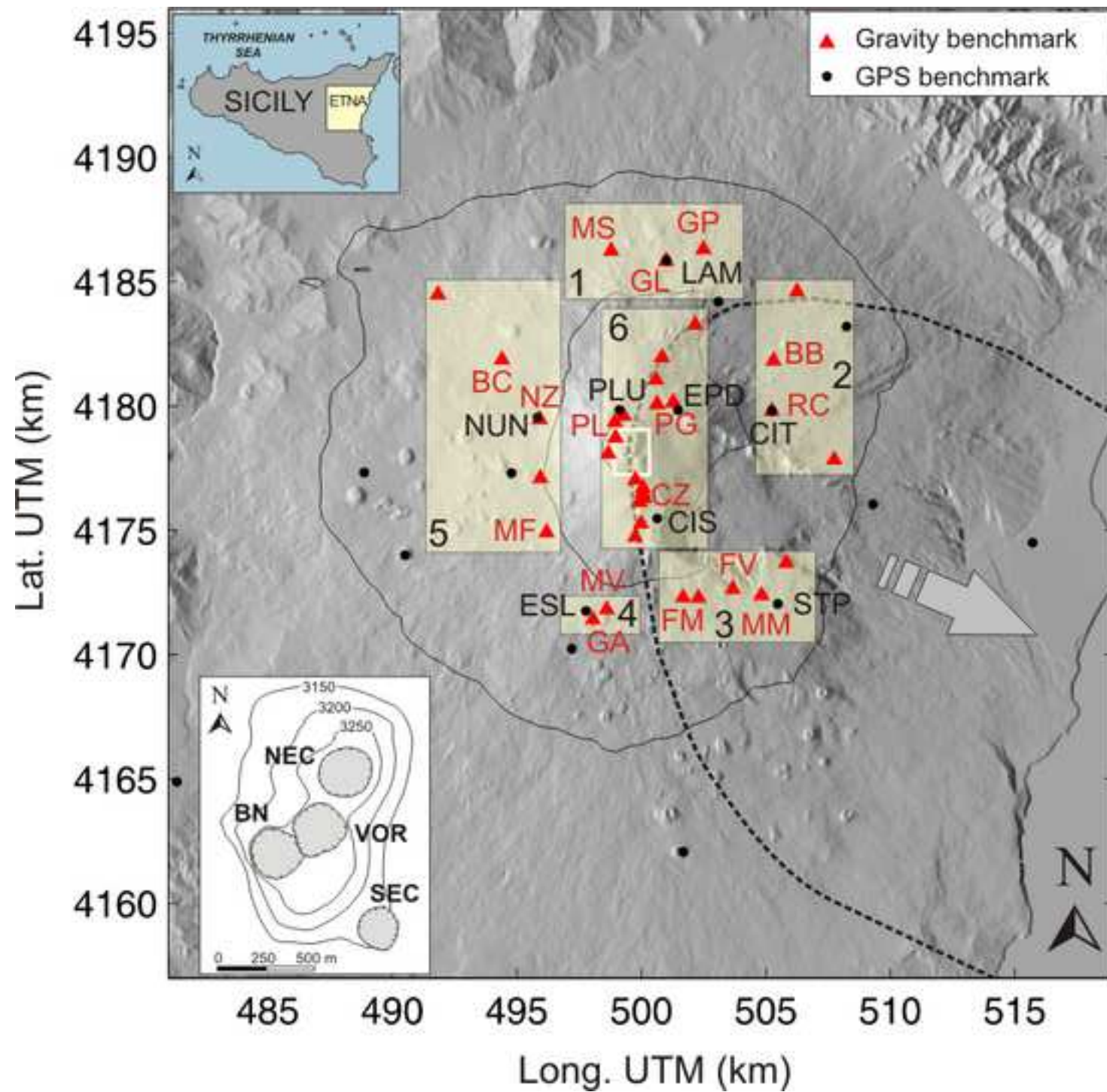


Figure 2  
[Click here to download high resolution image](#)

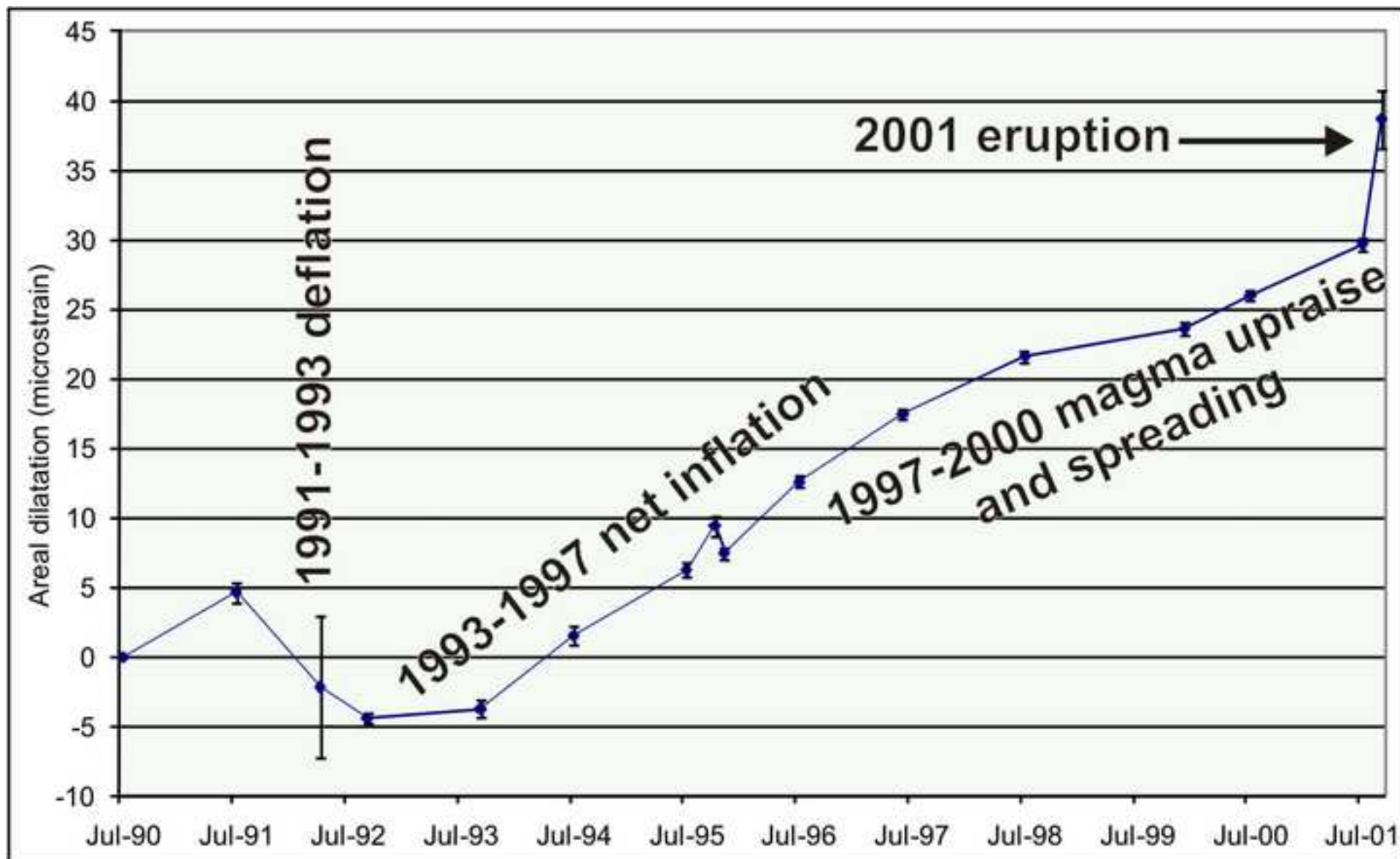


Figure 3  
[Click here to download high resolution image](#)

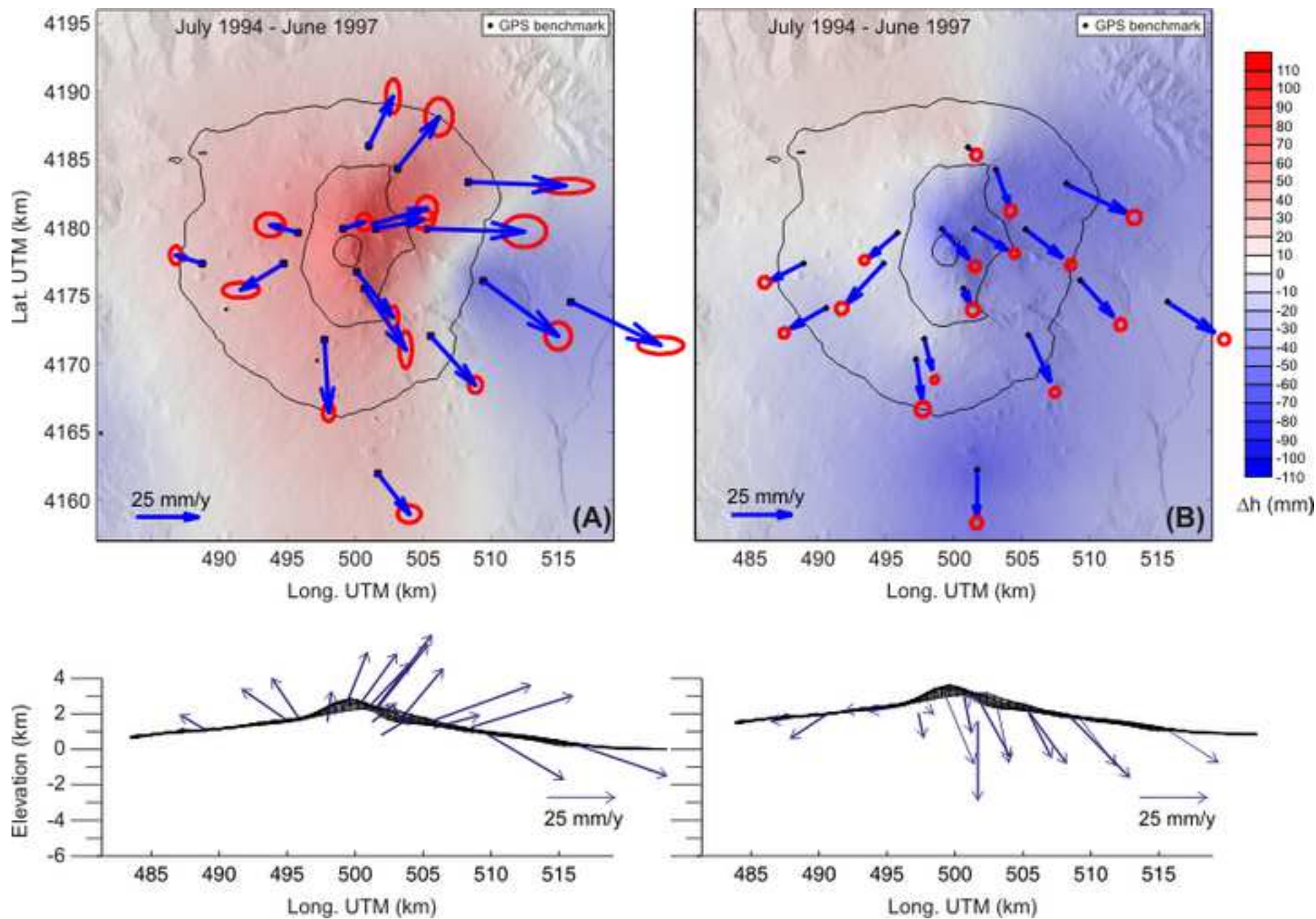


Figure 4  
[Click here to download high resolution image](#)

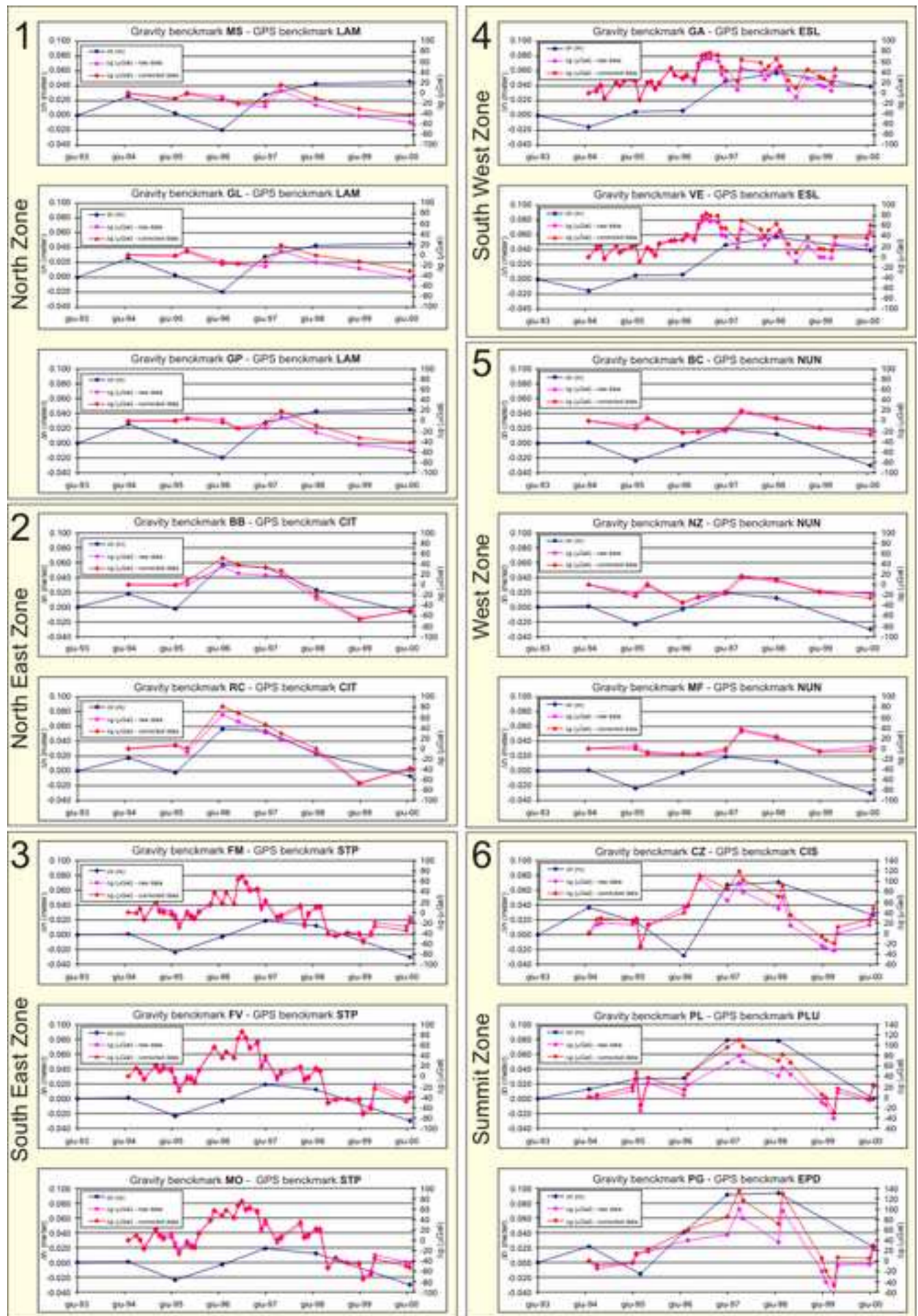


Figure 5  
[Click here to download high resolution image](#)

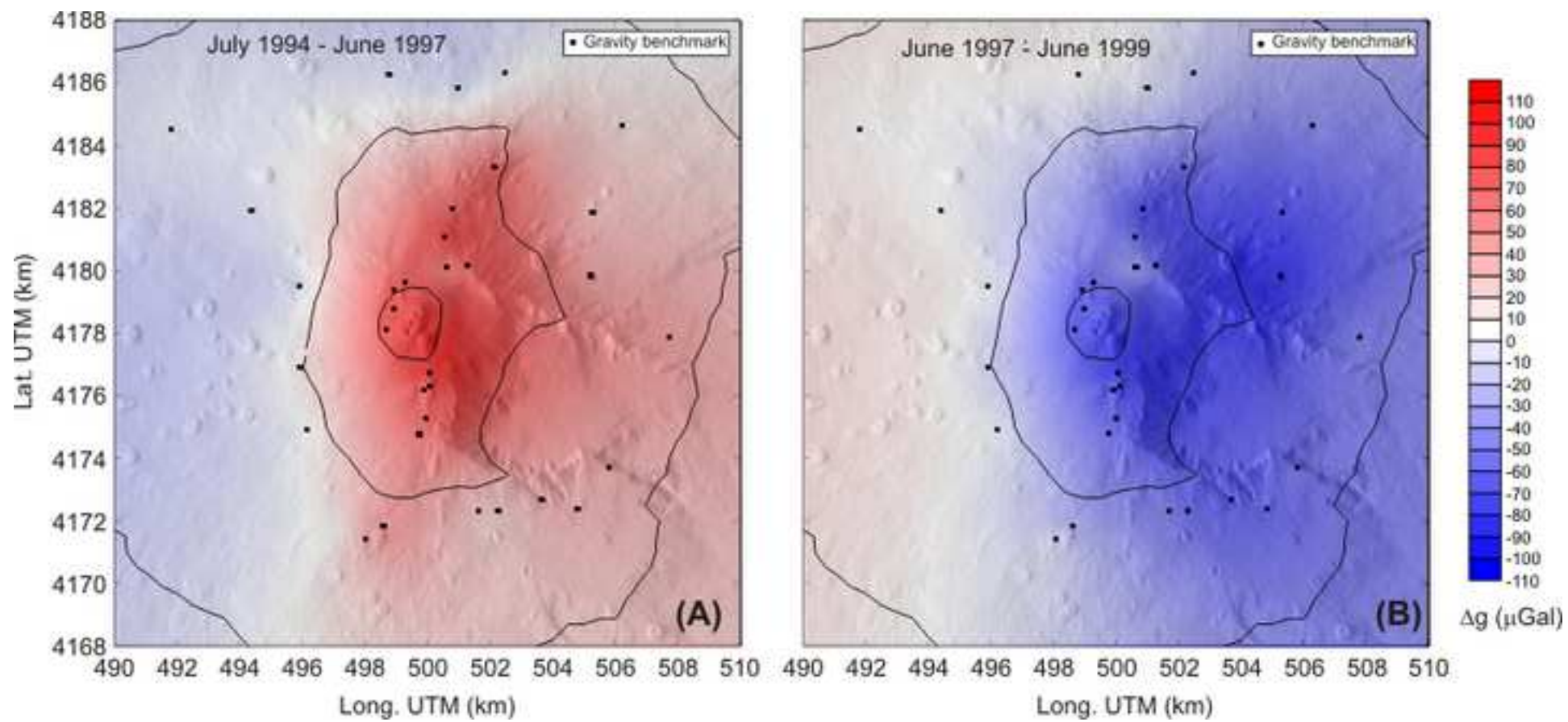


Figure 6  
[Click here to download high resolution image](#)

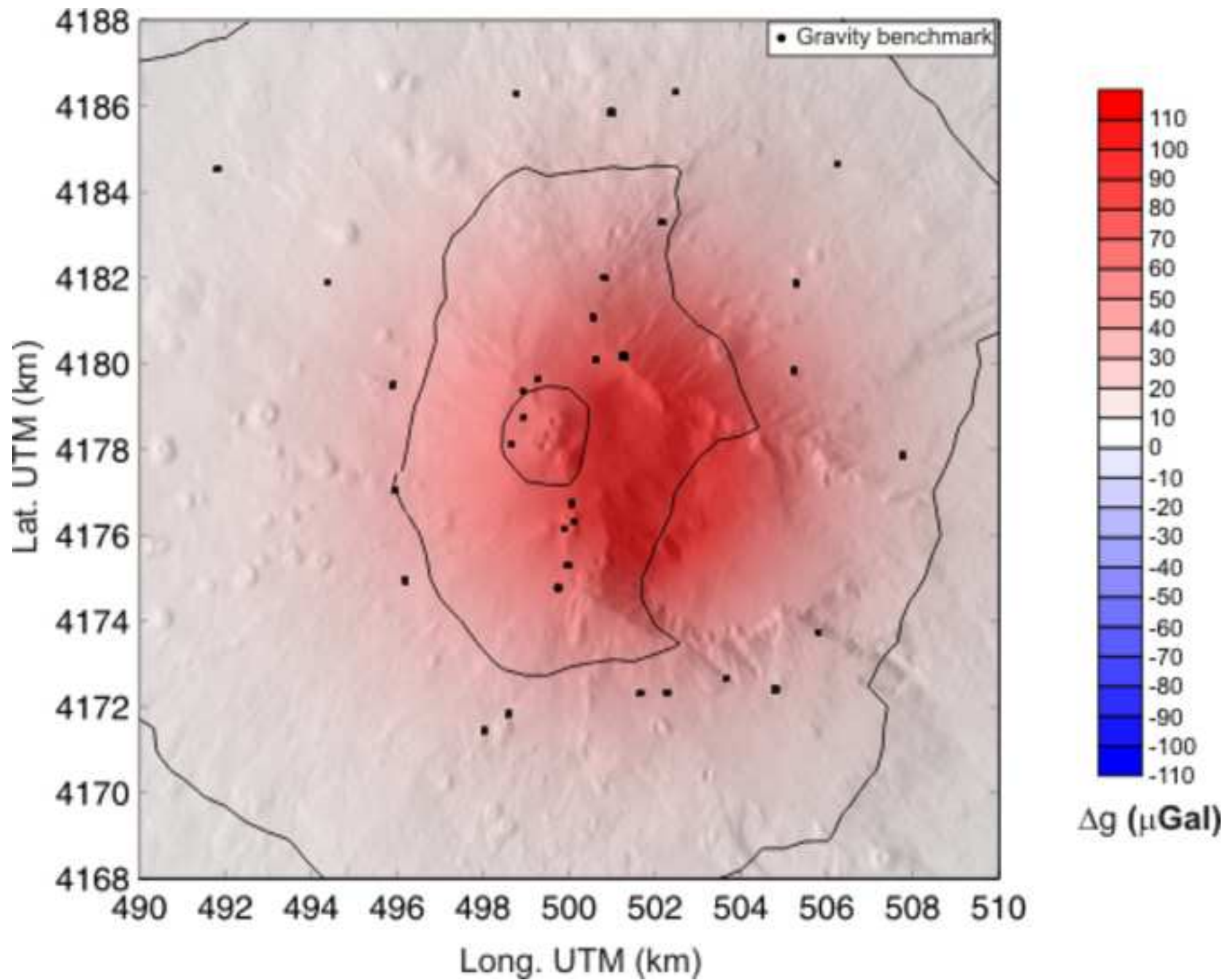


Figure 7  
[Click here to download high resolution image](#)

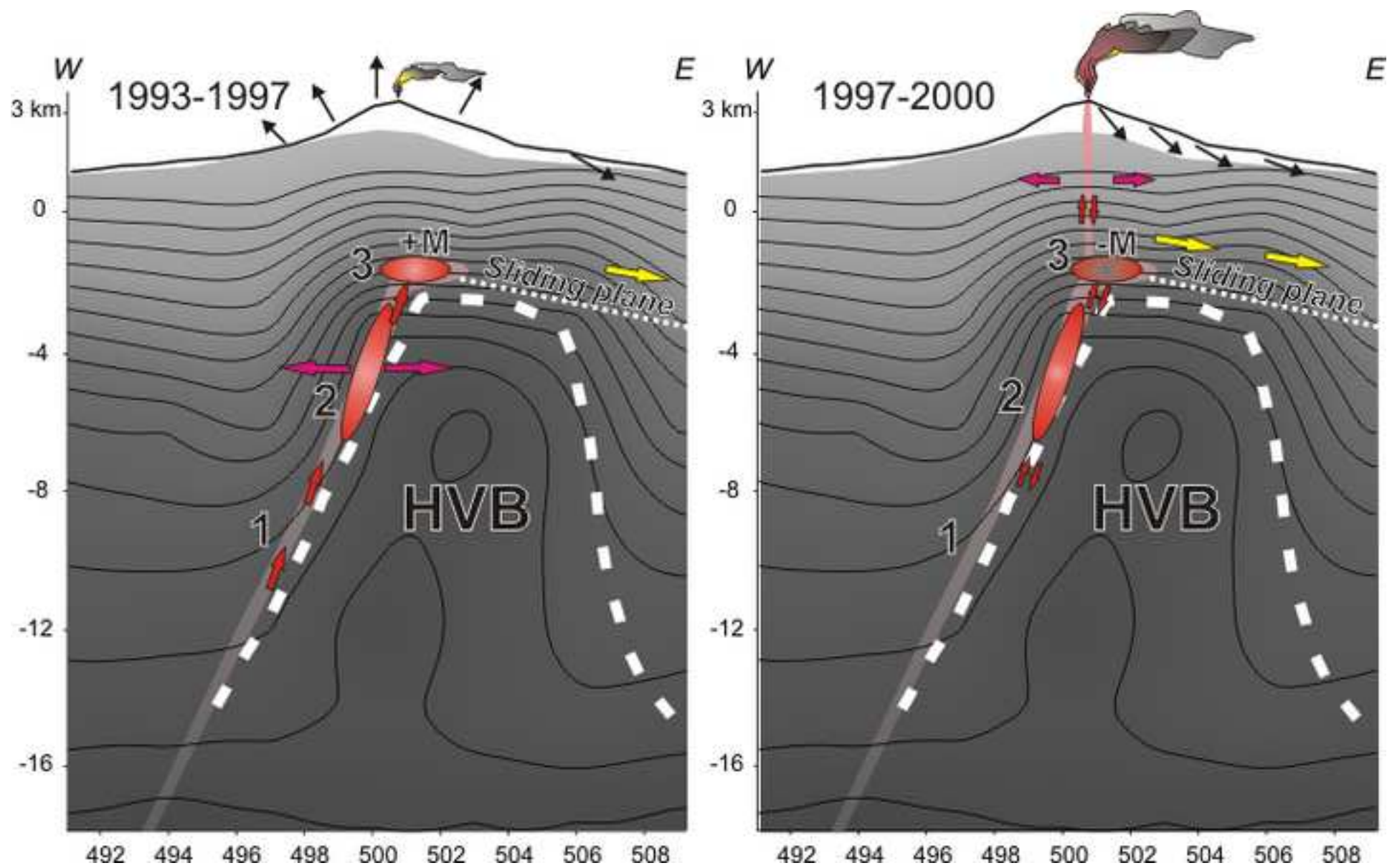


Table 1

[Click here to download Table: Table\\_1.doc](#)

1

<b>Geometry</b>	<b>Sphere</b>	<b>Prism</b>	<b>Cylinder</b>	<b>Ellipsoid</b>
Xc – Easting (m)	501189	501151	501151	501171
Yc – Northing (m)	4177624	4177805	4177821	4177816
Zc – Center depth (m)	-1820	-2160	-2480	-2300
L - Length (m)		2880		
W – Width (m)		1770	3320	
$\phi$ - Azimuth (from the North)		-21°		
R - radius (m)			310	
a – semi-major axis (m)				1360
b - semi-minor axis (m)				300
<b>1994-1997</b>				
U* $\Delta\rho$ – thickness* density (kg/m <sup>2</sup> )		6.4*10 <sup>4</sup>		
$\Delta\rho$ - density (kg/m <sup>3</sup> )			350	390
$\Delta M$ - mass change (kg)	3.2*10 <sup>11</sup>	3.4*10 <sup>11</sup>	3.5*10 <sup>11</sup>	3.5*10 <sup>11</sup>
Misfit ( $\mu$ Gal)	19.37	18.95	19.04	18.99
<b>1997-1999</b>				
U* $\Delta\rho$ – thickness* density (kg/m <sup>2</sup> )		-7.23*10 <sup>4</sup>		
$\Delta\rho$ - density (kg/m <sup>3</sup> )			-360	-320
$\Delta M$ - mass change (kg)	-3.5*10 <sup>11</sup>	-3.7*10 <sup>11</sup>	-3.6*10 <sup>11</sup>	3.8*10 <sup>11</sup>
Misfit ( $\mu$ Gal)	26.71	25.74	25.86	25.85

2

3

4

5

**Table 1**



**Table 2**[Click here to download Table: Table\\_2.doc](#)1  
2  
3

<b>Period</b>	<b>Activity</b>	<b>Volume (x10<sup>6</sup> m<sup>3</sup>)</b>
1995-97	Strombolian activity and paroxysmal episodes, lava overflows	7
1998	Strong explosive activity, lava fountains, lava overflow	8
1999 (Feb-Nov)	Summit effusive eruption	25
1999 (Jun-Oct)	Strong explosive activity, several episodes of lava fountains, extensive lava flows	20
2000	66 fire paroxysmal eruptive episodes with lava fountains and extensive lava flows	47
2001 (Jan-Jul)	Strombolian activity, 16 paroxysmal eruptive episodes with extensive lava flows	12
2001 (Jul-Aug)	Flank eruption – effusive and explosive activity	40
2002-03	Flank eruption – effusive and explosive activity	52

4